Contract No:

This document was prepared in conjunction with work accomplished under Contract No. DE-AC09-08SR22470 with the U.S. Department of Energy (DOE) Office of Environmental Management (EM).

Disclaimer:

Vertical Bridgman growth and characterization of $Cd_{0.95-x}Mn_xZn_{0.05}Te$ (x=0.20, 0.30) single-crystal ingots

V. Kopach[a], O. Kopach[a], L. Shcherbak[a], P. Fochuk[a], S. Filonenko[b], A. E. Bolotnikov[c], R. B. James[d]
[a]Chernivtsi National University, Ukraine;
[b]L.V. Pisarzhevskii Institute of Physical Chemistry of NAS of Ukraine, Ukraine;
[c]Brookhaven National Laboratory, USA;
[d]Savannah River National Laboratory, USA

ABSTRACT

Solid-liquid phase transitions in $Cd_{0.95-x}Mn_xZn_{0.05}Te$ alloys with x = 0.20 and 0.30 were investigated by differential thermal analysis (DTA). The heating/cooling rates were 5 and 10 K/min with a melt dwell time of 10, 30 and 60 minutes. $Cd_{0.95-x}Mn_xZn_{0.05}Te$ (x=0.20, 0.30) single-crystal ingots were grown by the vertical Bridgman method guided by the DTA results.

Te inclusions (1-20 micron diameter), typical of melt-grown CdTe and Cd(Zn)Te crystals, were observed in the ingots by infrared transmission microscopy. The measured X-ray diffraction patterns showed that all compositions are found to be in a single phase. Using current-voltage (I-V) measurements, the resistivity of the samples from each ingot was estimated to be about 10^5 Ohm·cm. The optical transmission analysis demonstrated that the band-gap of the investigated ingots increased from 1.77 to 1.88 eV with an increase of the MnTe content from 20 to 30 mol. %.

Keywords: Differential thermal analysis (DTA), $Cd_{0.95-x}Mn_xZn_{0.05}Te$, Bridgman technique, semi-magnetic semiconductor, cluster volume fraction, XRD.

1. INTRODUCTION

Currently diluted magnetic semiconductors generate increasing interest of scientists because of their unique properties: 1) the band-gap and lattice parameters can be varied by changing the composition of the solid solution; 2) the specific magnetic properties such as spin transitions at low temperatures in disordered magnetic alloys; 3) the presence of magnetic ions Mn^{2+} leads to spin-spin exchange interaction, which affects the electrical parameters; 4) the Mn-containing semiconductors can be used as detectors of infrared radiation and as light modulators in the visible and infrared regions [1].

$Cd_{1-x}Mn_xTe$ is the most studied of dilute magnetic semiconductors due to its optical, magnetic, magneto-optical and transport properties [2]. This compound has a structure of sphalerite (zinc blende) with $0 \le x \le 0.7$ [3]. $Cd_{1-x}Zn_xTe$ has long been known to have great potential in room-temperature X-ray and gamma-ray semiconductor detector applications [4]. Therefore, it is of a great interest to try to combine both semiconductors by growth of the diluted magnetic semiconductor $Cd_{1-x-y}Mn_xZn_yTe$.

Previously, we studied peculiarities of melting and crystallization processes of diluted $Cd_{1-x-y}Mn_xZn_yTe$ magnetic semiconductors belonging to a quasi ternary system ZnTe–CdTe–MnTe [5, 6] by differential thermal analysis (DTA). The goal of the present work is to enlarge the manganese content from x=0.2 to 0.3 at the same Zn concentration and determine the physico-chemical properties of the single crystals grown by vertical Bridgman method.

2. EXPERIMENTS

To carry out the DTA of $Cd_{0.95-x}Mn_xZn_{0.05}Te$ alloys (x=0.20 and 0.30), samples (mass of 5 g) were synthesized from high-purity materials of Cd, Zn, Te (6N) and Mn (5N) in a glassy carbon crucible placed in a quartz ampoule. The last was sealed under a pressure of $4x10^{-4}$ mbar and was placed in a vertical furnace where the synthesis process occurred over 8 hours. Then samples for DTA were prepared by evacuating 500 mg of these alloys in a graphite-coated quartz ampoule (d = 8 mm). The ampoules were sealed under pressure of $4x10^{-4}$ mbar. The DTA was performed with heating-cooling rate equal to 5 and 10 K/min with an intermediate melt dwell time of 10, 30 and 60 min. Using this method we determined the temperatures of the solid-liquid phase transition of $Cd_{0.95-x}Mn_xZn_{0.05}Te$ alloys, the melt superheating

(ΔT^+) and supercooling (ΔT^-) values, the solid-state phase volume fraction ($\varphi_{clusters}$), and the solidification rate ($V_{sol.}$, sec^{-1}).

$Cd_{0.95-x}Mn_xZn_{0.05}Te$ (CMZT-1 and CMZT-2 with x=0.20 and 0.30, respectively) single-crystal ingots were grown by a two-step process, namely, synthesis in the glassy carbon crucible following by the vertical Bridgman method growth. The synthesized materials were loaded to the graphite-coated quartz ampoule and sealed under a pressure of $4x10^{-4}$ mbar. The crystal growth was carried out in a two-zone furnace with the lowering rate of 2.8 mm/h along a temperature gradient of 13 K/cm. As a result the CMZT-1 and CMZT-2 single-crystal ingots with a diameter of 16 mm and length of 35 and 37 mm, respectively, were obtained.

2-mm-thick wafers were sliced perpendicular to the crystal axis in the as-grown CMZT-1 and CMZT-2 ingots. All the wafers were mechanically polished with 1, 0.3 and 0.05 mm particle size alumina oxide suspension and then chemically polished with 5% bromine–methanol solution.

The crystalline nature of the samples was verified by the powder XRD patterns using a DRON-3M X-Ray generator. To study the resistivity the current-voltage, I-V curves were measured using a Keithley 617 electrometer. The optical analysis was performed by the transmission method using an Ocean Optics OO-2000 Spectrometer.

3. RESULTS AND DISCUSSIONS

3.1 Differential thermal analysis

Similar to earlier studies of [5, 6] $Cd_{0.95-x}Mn_xZn_{0.05}Te$ alloys with x= 0.05 and 0.15, the solid solutions CMZT-1 and CMZT-2 were melted in certain temperature intervals regulated by the specimen's heating rate. As a rule the alloy crystallization occurred with supercooling in relation to the melting temperature. To provide full homogenization the melt was maintained for some time at a set temperature (superheating) following by cooling at a certain rate.

Fig. 1 demonstrates the DTA results of supercooling versus its superheating for $Cd_{0.75}Mn_{0.20}Zn_{0.05}Te$ and $Cd_{0.65}Mn_{0.30}Zn_{0.05}Te$ alloys. The superheating ΔT^+ and the supercooling ΔT^- values were estimated as:

$$\Delta T^+ = T_{dwell} - T_{start.\ melt} \quad (1)$$

$$\Delta T^- = T_{start.\ melt} - T_{start.\ sol}, \quad (2)$$

where T_{dwell} is the superheating melt-dwell temperature, $T_{start\ melt}$ is the temperature at the beginning of the alloy melting, and $T_{start\ sol}$ is the temperature at the beginning of the melt solidification.

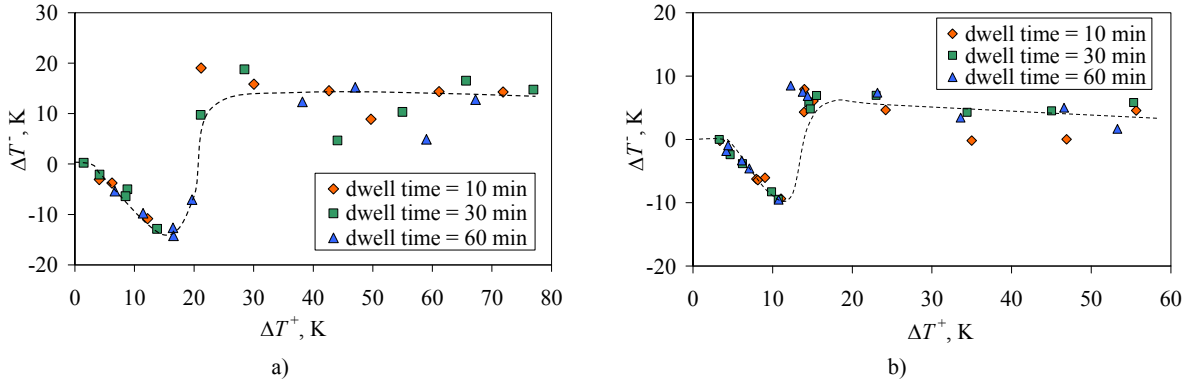

Figure 1. The supercooling versus superheating dependences for (a) the $Cd_{0.75}Mn_{0.20}Zn_{0.05}Te$ and (b) the $Cd_{0.65}Mn_{0.30}Zn_{0.05}Te$ alloys ($V_{h/c}$ = 5 K/min).

According to the data in Fig. 1, both melts crystallized with supercooling when they were superheated above 20 K (CMZT-1) or 10 K (CMZT-2) in comparison to $T_{start.\ melt.}$ However, a zone with "negative" supercooling effect ($\Delta T^- < 0$) is evident for both slightly superheated alloys. So, at first sight the melts' crystallization temperatures are higher than the alloys' start-melting temperatures ("negative" supercooling effect). It means that solid phase particles (clusters) are still present in such melts, which act as centers of crystallization at further melt cooling. The supercooling value for the CMZT-1 (Fig.1(a)) is about 12±5 K, while for the sample CMZT-2 (Fig. 1 (b)), it is less than 10 K after superheating

above the critical point of liquidus. Thus, the melt supercooling value of the samples decreases with increasing MnTe content in the alloys. Such dependence was also observed in our previous studies [5, 6].

A higher degree of superheating (above some critical points) for melts trends toward higher supercoolings, because solid-like particles had melted fully resulting in the absence of nuclei. Owing to local fluctuations of the component concentrations in the supercooling melts, lots of nuclei appear during the next melt-cooling process.

It is well-known that mixtures tend to melt and solidify over a temperature range, and they start to melt or solidify at one temperature and do not complete the process until they reach an upper or lower point (of liquidus or solidus lines). To define the temperature range of solid-liquid phase coexistence and kinetics of the melt homogenization, we used a series of DTA experiments with a melt dwell-time duration of 10 - 60 min. Fig. 2 presents the temperature dependencies of the volume fraction of the solid-like phase ($\varphi_{clusters}$) remaining in CMZT-1 (Fig. 2 (a)) and CMZT-2 (Fig. 2 (b)) melts.

The melting process of $Cd_{0.75}Mn_{0.20}Zn_{0.05}Te$ alloy starts at 1342 K and ends at 1373 K, while for $Cd_{0.65}Mn_{0.30}Zn_{0.05}Te$ alloys the melting range was 1346-1374 K. So, an increase in the MnTe content from 20 to 30 mol. % leads to a decrease in the temperature gap between the beginning and end of the melting process. Any influence of the melting process for these alloys on the dwell time was not obtained. Thus, two points of solidus and liquidus lines for the system CdTe – ZnTe – MnTe are determined. The liquidus and solidus sheets shrink from 31 to 28±1 K.

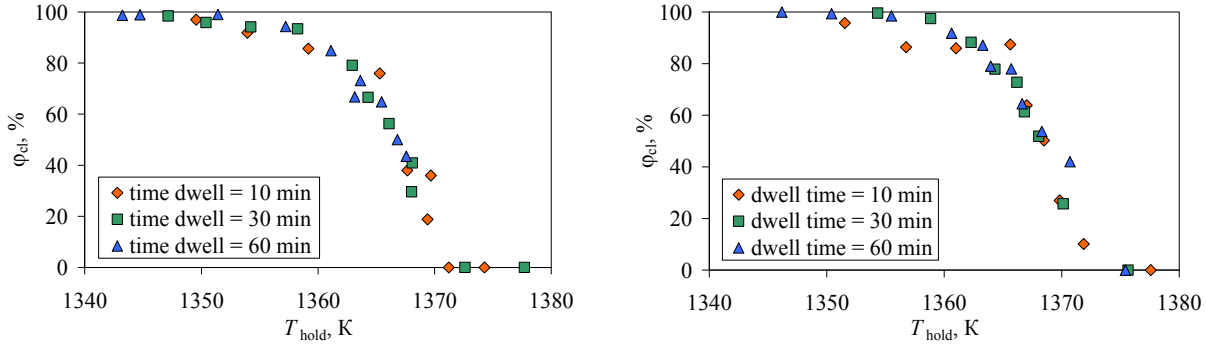

Figure 2. The temperature dependencies of the volume fraction of the solid phase remaining in $Cd_{0.75}Mn_{0.20}Zn_{0.05}Te$ (a) and $Cd_{0.65}Mn_{0.30}Zn_{0.05}Te$ (b) melts ($V_{h/c}$ = 5 K/min).

DTA data allow us to compare the velocity of the melts nucleation following by the nuclei growth and melt crystallization. The solidification rate ($V_{sol.}$,sec^{-1}) was defined as a reciprocal time of record of the melt's crystallization exothermic process in the thermograms.

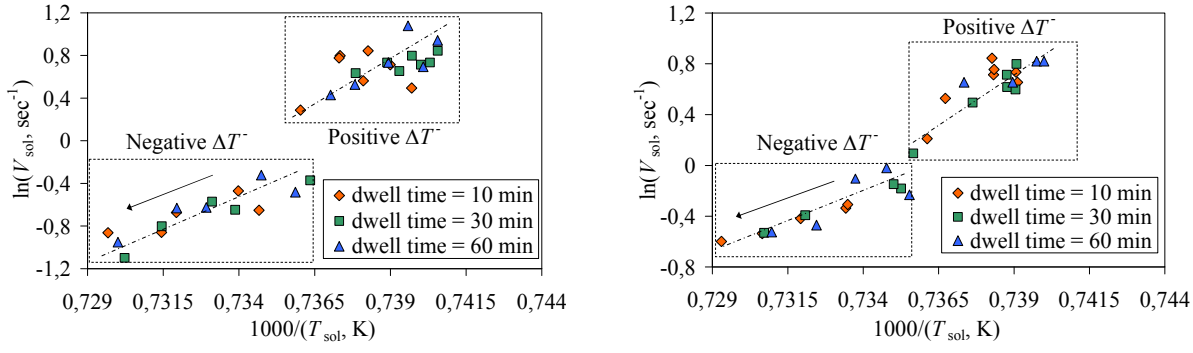

Figure 3. Crystallization-rate logarithm versus reciprocal crystallization temperatures for the $Cd_{0.65}Mn_{0.30}Zn_{0.05}Te$ alloy with $V_{h/c}$ = 5 K/min (a) and $V_{h/c}$ = 10 K/min (b).

The dependence of the crystallization rate versus crystallization temperature (T_{sol}) for the CMZT-1 alloy (Fig. 3 (a) and (b)) demonstrates that the high supercooled melt solidified faster (as a rule, spontaneously). Thus, the increase in the crystallization temperature is accompanied by a decrease in the crystallization rate. Semi-logarithmic plots of the dependence clearly revealed two slopes in the temperature range, designated for convenience as zones with "negative" and "positive" supercooling. The arrows in Fig. 3 correspond to the direction of the increase in superheating.

The slope at $V_{h/c}$ = 5 K/min can be described by Eqs. 3 and 4 for "negative" and "positive" supercooling zones, respectively:

$$\ln V_{sol} = 91835 \cdot T^{-1} - 67.96 \quad (3)$$

$$\ln V_{sol} = 79360 \cdot T^{-1} - 57.93 \quad (4)$$

Reduced equilibrium conditions for crystallization (higher the melt cooling rate, $V_{h/c}$ = 10 K/min, Fig. 3 (b)) leads to a more observable difference in the dependence slope that can be described by

$$\ln V_{sol} = 84060 \cdot T^{-1} - 61.94 \quad (5)$$

$$\ln V_{sol} = 143220 \cdot T^{-1} - 105.11 \quad (6)$$

The increase in dwell duration from 10 to 60 min does not cause significant changes.

An analysis of Eqs. 3-6 leads to the conclusion that crystallization of a more homogeneous (high superheated) liquid requires a higher activation energy for the nucleation process. Analogous to the Eq. 6 dependence,

$$\ln V_{sol} = 147509 \cdot T^{-1} - 107.68 \quad (7)$$

was obtained in a case of the binary only CdTe melt in [7]. Obviously the nucleation in the quaternary alloy melt occurs based on the major component participation, i.e., CdTe. There are solid-like particles that remain in slightly superheated melts; these particles acts as nuclei, which increase in size during cooling and when the speed of the process is not too high (negative supercooling region in Fig. 3). So, for less solid-like particles and more liquid in melt, the crystallization process takes more time, which results in a decrease in the crystallization rate. Higher superheatings (above critical points) trends toward higher supercoolings, because the nucleus formation in the disordered liquid occurs by overcoming an energy barrier.

3.2 Crystal Structure

Fig. 4 depicts the as-grown crystals with x=0.20 and 0.30, respectively. The wafers were cut perpendicular to the ingot's axis (Fig. 5). Both the crystals are single grain with a large number of twins. Our work is in agreement with the analyses of the morphology and crystallography of twins in $Cd_{1-x}Mn_xTe$ (x=0.2) crystals in [8, 9] and heavily twinned crystals with x = 0.20 and 0.35 in [3]. Thus, 0.05 mol. % of Zn has no influence on twins formation in the process of CMZT-1 and CMZT-2 crystal growth.

a) b)

Figure 4. Photographs of as-grown CMZT-1 (lower part was cut off) (a) and CMZT-2 (b).

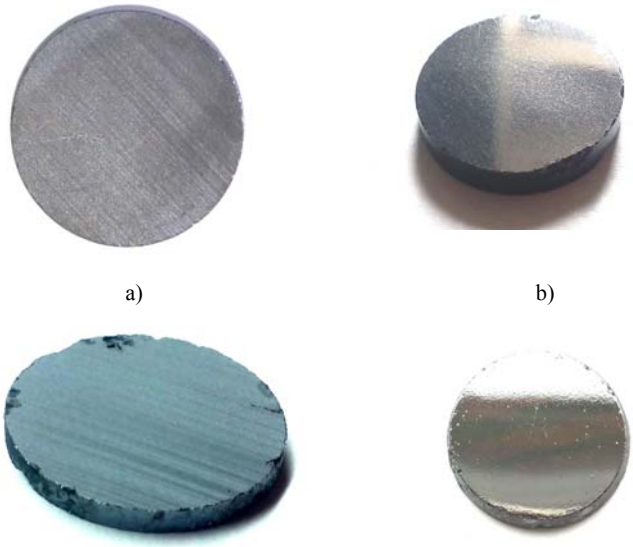

a) b)

c) d)

Figure 5. Photographs of the wafers CMZT-1 (g = 0.4) (a, b) and CMZT-2 (g = 0.3) (c, d) cut perpendicular to ingot's axis. The wafers b and d were chemically polished.

The infrared microscopy determined a high content of nontransparent inclusions in the ingots. A typical IR image of Te inclusions (similar to Cd(Zn)Te crystals) in CMZT-1 is shown in Fig. 6. Spherical-like inclusions with a size of 1-20 μm are randomly distributed in the crystal.

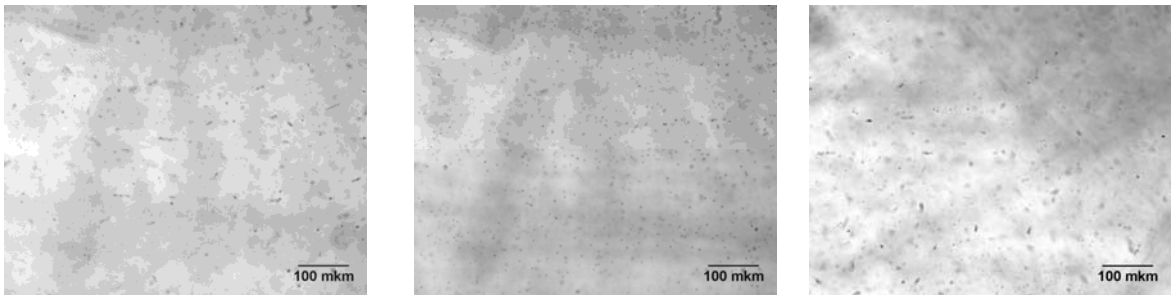

a) b) c)

Figure 6. IR transmission microscopy images showing the Te precipitates in $Cd_{0.75}Mn_{0.20}Zn_{0.05}Te$ (g= 0.1 (a), 0.4 (b), 0.9 (c)).

Similar features were observed in CMZT-2 wafers. Fig. 7 represents typical IR transmission image with, most likely, the presence of Te precipitates or inclusions in CMZT-2 ingot. Imperfections with 1-20 μm diameter were also determined. However the precipitates show a tendency for ordering in quasi-parallel lines and along stacking faults formation that can be caused by a lateral mechanism in the crystal growth process. Besides, "drops" of lighter than matrix phase Ø (up to 50-μm size) can be seen in the image.

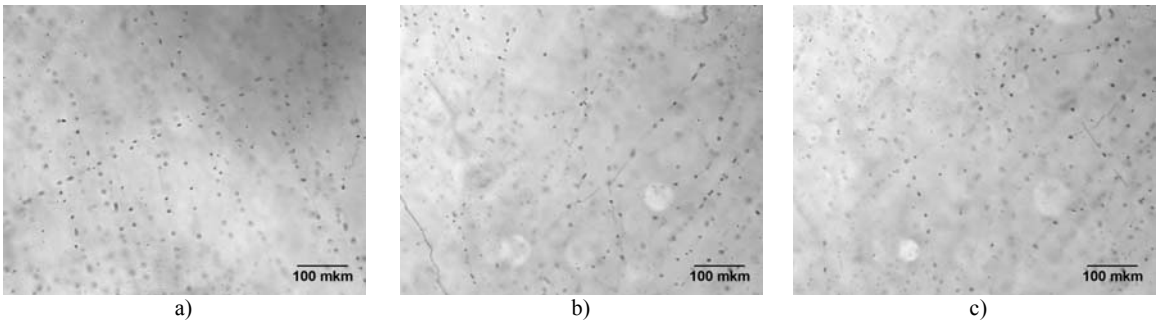

a) b) c)

Figure 7. Typical IR transmission microscopy images showing the Te inclusions/precipitates in $Cd_{0.65}Mn_{0.30}Zn_{0.05}Te$ (g= 0.1 (a), 0.3 (b), 0.8 (c)).

The powder X-ray diffraction patterns using Cu-Kα (λ=1.542) radiation for samples taken from different parts of CMZT-1 are shown in Fig. 8 (a). The range of scanning angle was from 20 to 80°.

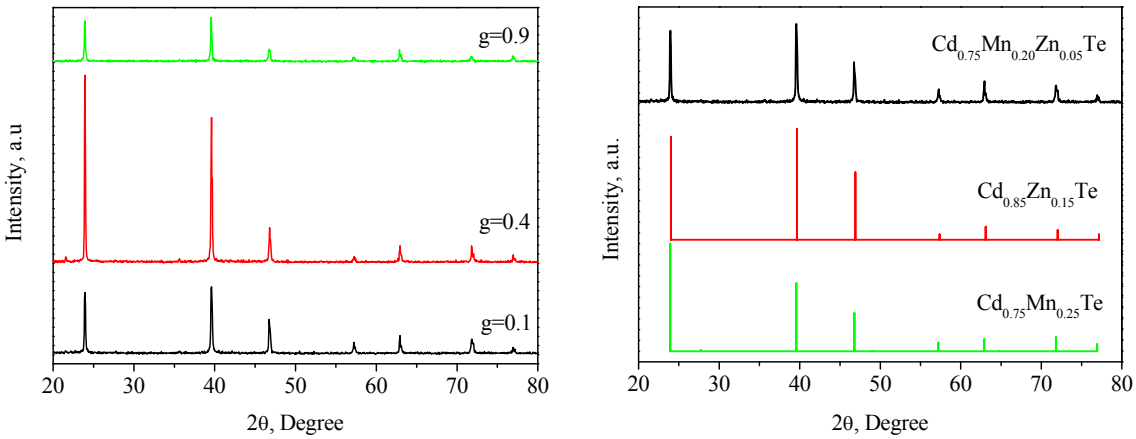

a) b)

Figure 8. XRD patterns of an as-grown $Cd_{0.75}Mn_{0.20}Zn_{0.05}Te$ crystal (g= 0.1; 0.4 and 0.9) (a). Standard patterns of $Cd_{0.75}Mn_{0.25}Te$ [10] and $Cd_{0.85}Zn_{0.15}Te$ [11] (b) are given for comparison.

The observed X-ray data showed that all compositions are single-phase. Compared to the data for g=0.1 and g=0.9, the intensity of the diffraction peaks for g=0.4 shifts toward the higher values. This can be explained by the fact that the Mn content in the middle part of the ingot is slightly lower than at the beginning and at the top of the crystal. It is known [12, 13] that the segregation coefficient of Mn in CdTe crystals is equal to near unity, while the k_{eff} (Zn) value in $Cd_{0.98}Zn_{0.02}Te$ is estimated to be 1.16 and even as high as 1.3 [14]. Obviously, the small addition of Zn slightly influenced the quarternary crystal lattice parameters along the crystal axis resulting in Zn-content and Mn-content inhomogeneities.

The powder X-ray diffraction patterns for all the samples are in good agreement with the standard patterns of $Cd_{0.75}Mn_{0.25}Te$ and $Cd_{0.85}Zn_{0.15}Te$ (Fig. 8 (b)), which belong to the cubic structure with lattice parameters a = 6.44 Å and a = 6.42 Å, respectively (ICDD data base PDF 03-065-8866 and 00-053-0552). The Miller indices (*hkl*) of the lattice planes are (111), (220), (311), (400), (331), (422) and (511) for the $Cd_{0.75}Mn_{0.25}Te$ and (111), (220), (311), (400), (331), (422) and (333) for the $Cd_{0.85}Zn_{0.15}Te$. Diffraction peaks for other phases, such as metallic Cd, Te, Zn, Mn or their oxides states, were not observed.

3.3 Optical and electrical properties

Typical optical transmission spectra of as-grown CMZT-1 and CMZT-2 crystal ingots are shown in Fig. 9. The data indicate that substitution in cation sublattices by manganese atoms causes broadening of the fundamental edge from 1.77

to 1.88 eV. Some shift in the E_g value along the axis in both ingots leads to the conclusion about segregation of Mn during the directed solidification process with a segregation coefficient different from unity. Relatively low transient about 40-50 % in the specimens could be connected with the high content of Te precipitates shown in Figs. 6 and 7.

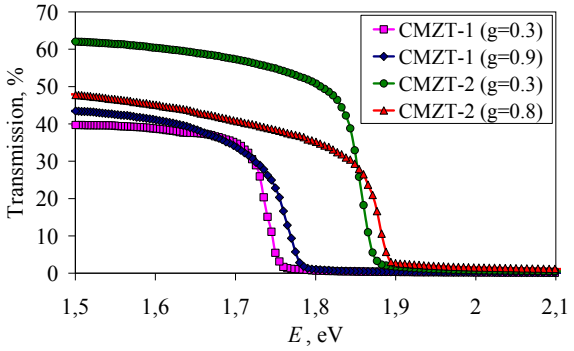

Figure 9. Typical transmission spectra of as-grown CMZT-1 and CMZT-2 crystals.

The as-grown CMZT-1 and CMZT-2 samples were selected after mechanical and chemical polishing to fabricate an acceptable structure for electrical characterization. Gold was deposited for contact metallization. Current–voltage (I–V) curves of the as-grown CMZT-1 and CMZT-2 crystals under bias voltages from -10 to 10 V are shown in Fig. 10. It is evident that the behavior of the I-V curves is linear at low voltages at room temperature.

The resistivity was calculated from the measured I–V curves using the equation:

$$\rho = R \cdot S/l, \tag{8}$$

where R is the resistance of the sample, S the contact area, and l is the thickness. The electrical resistivity ρ obtained from the I–V curves was $2x10^5$ Ohm-cm for CMZT-1 and $5x10^4$ Ohm-cm for CMZT-2.

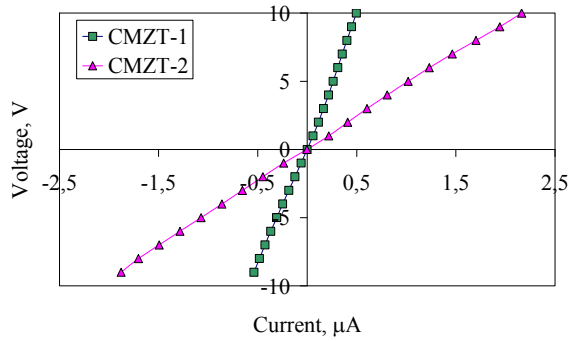

Figure 10. I–V curve of the as-grown CMZT-1 (g= 0.3) and CMZT-2 (g= 0.3) crystals under bias voltages from -10 to 10 V.

These values mean that the sputtered Au film can form a good ohmic contact to Cd(Mn,Zn)Te crystal, but the resistivity value needs to be improved by doping with compensating elements, e.g. In, Al, V, which act as donors in the crystal similar to their role in Cd(Zn)Te and Cd(Mn)Te ingots. During the growth process of Cd(Mn,Zn)Te crystal by vertical Bridgman method from stoichiometric source material similar to Cd(Mn)Te [15], a large number of Cd atoms escape from the ingot due to its high vapor pressure at the high growth temperature, leaving a lot of Cd vacancies (V_{Cd}) in the as-grown crystal, which act as acceptor centers and decrease the resistivity.

Based on the resistivity values it is clear that crystal CMZT-2 has a lower resistivity compared to the crystal CMZT-1. The lowering of the resistivity is likely due to more uniform distribution of the components (and impurities) in the original melt at higher temperatures.

4. CONCLUSIONS

$Cd_{0.95-x}Mn_xZn_{0.05}Te$ alloys (x=0.20 and 0.30) were investigated by a DTA method. We found that for an increase of the MnTe content in the alloys, the supercooling value of the sample decreases. Moreover, the changing of the MnTe content from 20 to 30 mol. % decreased the melting temperature range. In the next step we grew $Cd_{0.95-x}Mn_xZn_{0.05}Te$ (x=0.20, 0.30) single-crystal ingots by the vertical Bridgman method. The observed X-ray diffraction patterns showed that all compositions have a single phase. Te inclusions were observed in both ingots, and the majority have a spherical shape with a diameter of 1-20 μm. The optical transmission spectra revealed that an increase in the composition of MnTe from 20 to 30 mol. % resulted in an increase in the band-gap E_g from 1.77 to 1.88 eV. However, the electrical resistivity for CMZT-1 sample was $2x10^5$ Ohm-cm, and for CMZT-2 sample it was found to be only $5x10^4$ Ohm-cm, indicating the need for a compensating dopant for use of the material as an X-ray or gamma-ray detector.

REFERENCES

[1] De Melo, O., Leccabue, F., Panizzieri, R., Pelosi, C., Bocelli, G., Calestani, G., Sacredo, V., Chourio, M. and Paparazzo, E., "CVT growth, thermodynamic and magneto-structural study of $Cd_{1-x}Mn_xTe$ single crystals," J. Crystal Growth 104, 780-788 (1990).

[2] Triboulet, R., Didier, G., "Growth and Characterization of $Cd_{1-x}Mn_xTe$ and MnTe crystals: contribution to the CdTe-MnTe pseudo-binary phase diagram determination," J. Crystal Growth 52, 614-618 (1981).

[3] Wu, A. Y. and Sladek, R. J., "Imperfections in the crystal structure of $Cd_{1-x}Mn_xTe$," J. Appl. Phys. 53, 85-89 (1982).

[4] Kim, K. H., Hwang, S., Fochuk, P., Nasi, L., Zappettini, A., Bolotnikov, A. E. and James, R. B., "The Effect of Low-Temperature Annealing on a CdZnTe Detector," IEEE Trans. Nucl. Sci. 63, 2278-2282 (2016).

[5] Kopach, V., Kopach, O., Fochuk, P., Shcherbak, L., Bolotnikov, A. and James, R. B., "Differential thermal analyses of $Cd_{0.95-x}Mn_xZn_{0.05}Te$ alloys," Proc. SPIE 8852, 88521D-1-5 (2013).

[6] Kopach, V., Kopach, O., Fochuk, P., Shcherbak, L., Bolotnikov, A. and James, R. B., "Kinetic parameters of $Cd_{1-x-y}Mn_xZn_yTe$ alloys melting and crystallization processes," Physica Status Solidi (C) 11, 1533-1537 (2014).

[7] Shcherbak, L., Feychuk, P., Kopach, O., Panchuk, O., Hayer, E., Ipser, H., "Fine structure of the melting process in pure CdTe and in CdTe with 2 mol % of Ge or Sn," J. Alloys Comp. 349, 145-149 (2003).

[8] Zhang, J., Jie, W., Wang, T., Zeng, D., Hao, Y., He, K., "Vertical Bridgman growth and characterization of CdMnTe substrates for HgCdTe epitaxy," J. Crystal Growth 310, 3203-3207 (2008).

[9] Zhang, J., Jie, W., Wang, L. and Luan, L., "Twins in CdMnTe single crystals grown by Bridgman method," Cryst. Res. Technol 45, 7-12 (2010).

[10] Abrahams, S. C., Marsh, P. and Bridenbaugh, P. M., "Atomic Substitution in $Cd_{1-x}Mn_xTe$ for $0.1 \leq x \leq 0.4$," Acta Cryst. 45, 545-548 (1989).

[11] Nkum, R. K., Weil, R., Muranevich, E., Benguigui, L., Kimmel, G., "X-Ray Diffraction Evidence for a Ferroelectric Phase Transition in Zinc Cadmium Telluride", Mater. Sci.Eng. B, B9, 217-219 (1991)

[12] Panchuk, O. and Fochuk, P., Doping. edited by Robert Triboulet and Paul Siffert: "CdTe and Related Compounds; Physics, Defects, Hetero- and Nano-structures, Crystal Growth, Surfaces and Applications" (Netherlands, 309-362, 2010).

[13] Hossain, A., Cui, Y., Bolotnikov, A., Camarda, G., Yang, G., Kim, K-H., Gul, R., Xu, L., Li, L., Mycielski, A. and James, R. B., "Cadmium Manganese Telluride ($Cd_{1-x}Mn_xTe$): A Potential Material for Room-Temperature Radiation Detectors," 51 Annual Meeting of the Institute of Nuclear Materials Management (INMM); Baltimore, 42, July 11-15, 1-11 (2010).

[14] Mycielski, A., Burger, A., Sowinska, M., Groza, M., Szadkowski, A., Wojnar, P., Witkowska, B., Kaliszek, W., Siffert, P., "Is the (Cd,Mn)Te crystal a prospective material for X-ray and γ-ray detectors? ," Physica Status Solidi (C) 2, 1585-1578 (2005).

[15] Zhang, J., Jie, W., Wang, T., Zeng, D., Ma S., Hua, H., Yang, B., "Crystal growth and characterization of $Cd_{0.8}Mn_{0.2}Te$ using Vertical Bridgman method," Materials Research Bulletin 43, 1239-1245 (2008).